Phyllosilicates formation in faults rocks: Implications for dormant fault-sealing potential and fault strength in the upper crust

Thibault Cavailhes, Roger Soliva, Pierre Labaume, Christopher Wibberley, Jean-Pierre Sizun, Claude Gout, Delphine Charpentier, Alain Chauvet, Bruno Scalabrino, Martine Buatier

▶ **To cite this version:**

Thibault Cavailhes, Roger Soliva, Pierre Labaume, Christopher Wibberley, Jean-Pierre Sizun, et al.. Phyllosilicates formation in faults rocks: Implications for dormant fault-sealing potential and fault strength in the upper crust. Geophysical Research Letters, 2013, 40 (16), pp.4272-4278. 10.1002/grl.50829 . hal-00903574

HAL Id: hal-00903574
https://hal.science/hal-00903574

Submitted on 11 May 2021

HAL is a multi-disciplinary open access archive for the deposit and dissemination of scientific research documents, whether they are published or not. The documents may come from teaching and research institutions in France or abroad, or from public or private research centers.

L'archive ouverte pluridisciplinaire **HAL**, est destinée au dépôt et à la diffusion de documents scientifiques de niveau recherche, publiés ou non, émanant des établissements d'enseignement et de recherche français ou étrangers, des laboratoires publics ou privés.

Phyllosilicates formation in faults rocks: Implications for dormant fault-sealing potential and fault strength in the upper crust

Thibault Cavailhes,[1,2] Roger Soliva,[1] Pierre Labaume,[1] Christopher Wibberley,[3] Jean-Pierre Sizun,[4] Claude Gout,[3] Delphine Charpentier,[4] Alain Chauvet,[1] Bruno Scalabrino,[5] and Martine Buatier[4]

Received 12 July 2013; revised 5 August 2013; accepted 5 August 2013; published 28 August 2013.

[1] Phyllosilicate content and related permeability of fault zones form primary controls on hydraulic and mechanical behavior of the brittle crust. Hence, understanding and predicting the localization of these ubiquitous minerals is a major issue for fundamental and applied geosciences. We describe normal fault zones cutting a foreland arkosic turbiditic formation suffering high-T diagenesis and formed under conditions (~200°C) typical of deeply buried reservoirs and common within the seismogenic interval. Microstructural analyses show a large proportion of phyllosilicates (up to 34%) in the fault rock, derived from near-complete feldspar alteration and disaggregation during deformation. This study shows that even faults with offsets (~20 cm) much lower than bed thickness can have such large feldspar-to-phyllosilicate transformation ratios, implying that the origin of the phyllosilicates is purely transformation related. These results imply that the potential sealing capacity and strength of faults could be predicted from the host rock feldspar content. Where sealing capacity and fault strength can be related to phyllosilicate content, these properties can then also be inferred from the predicted phyllosilicate content: this opens up new horizons concerning the hydraulic and the mechanical behavior of the upper crust. **Citation:** Cavailhes, T., R. Soliva, P. Labaume, C. Wibberley, J.-P. Sizun, C. Gout, D. Charpentier, A. Chauvet, B. Scalabrino, and M. Buatier (2013), Phyllosilicates formation in faults rocks: Implications for dormant fault-sealing potential and fault strength in the upper crust, *Geophys. Res. Lett.*, *40*, 4272–4278, doi:10.1002/grl.50829.

1. Introduction

[2] Understanding the constitution of fault zones in the upper crust is an important issue in (1) the mechanics and kinetics of deformations [e.g., *Scholz*, 1990; *Faulkner et al*., 2010], (2) the strength of faults [e.g., *Di Toro et al*., 2011], and (3) the characterization of geological reservoir partitioning [e.g., *Fisher and Knipe*, 2001]. The presence of phyllosilicates in fault zones is a critical parameter impacting membrane seal properties and rheological behavior of fault rocks and can drastically alter the static and dynamic strengths of faults [*Gapais*, 1989; *Moore and Byerlee*, 1989; *Wibberley and Shinamoto*, 2005; *Bradbury et al*., 2011]. This issue is particularly important in the 5–8 km depth interval, which corresponds to both the deeply buried reservoirs [*Fisher et al*., 2003] and common main earthquake initiation zone [*Maggi et al*., 2000] which are poorly known and of current scientific and industrial challenges.

[3] The phyllosilicate fraction in a fault zone results from mechanical incorporation [e.g., *Yielding*, 2002] and/or mineral changes during diagenetic/metamorphic reactions [*Mitra*, 1978; *Janecke and Evans*, 1988; *Evans*, 1990; *Kamineni et al*., 1993; *Wibberley*, 1999; *Wibberley and McCaig*, 1999; *Mullis et al*., 2002; *Haines and van der Pluijm*, 2012]. Although well described in the literature, feldspar muscovitisation and sericitization in fault zones has been observed in crystalline rocks, especially in subgreenschist-greenschist facies conditions, and within the sedimentary cover exhumed from 5–8 km depth interval [*Leclère et al*., 2012; *Cavailhes et al*., 2013]. However, the relative proportion between the mechanical versus chemical processes for incorporation of phyllosilicates in fault zones has never been quantified. This study quantifies the process of phyllosilicate formation during faulting in very low-grade metamorphism context.

2. Geologic Setting

[4] The studied faults cut the Grès d'Annot formation, a turbiditic succession deposited during the Priabonian-Rupelian in the SW Alpine foreland basin [*Joseph and Lomas*, 2004] (Figure 1). The Grès d'Annot formation was buried under the Embrunais-Ubaye nappes shortly after its deposition [*Kerckhove*, 1969] and exhumed during the Middle-Late Miocene by erosion associated with basement thrusting [*Labaume et al*., 2008]. The studied faults trend around N080°E–N100°E and are located in the Moutière-Restefond area, in the eastern part of the basin (Figure 1), where vitrinite reflectance measured on samples around the fault zones indicates maximal temperatures of 240–260°C; this suggests a burial depth around 8 km assuming a mean geothermal gradient of 30°C/km [*Labaume et al*., 2009]. The temperature of the studied fault zones during their growth was determined at about 200°C using thermodynamic modeling of synkinematic chlorite chemistry and microthermometry on fluid inclusions in quartz-calcite veins; this range of temperature is consistent with fault activity under 6–7 km of burial depth [*Leclère et al*., 2012; *Cavailhes et al*., 2013].

[1]Géosciences Montpellier, UMR 5243, Université Montpellier 2-CNRS, Montpellier CEDEX 5, France.
[2]Now at Badley Ashton & Associates Ltd., Winceby Ho Horncastle, United Kingdom.
[3]TOTAL, CSTJF, Pau, France.
[4]Chrono-Environnement, UMR 6249, Université de Franche-Comté-CNRS, Besançon, France.
[5]Géosciences Azur, UMR 7329, Université de Nice Sophia-Antipolis, Valbonne, France.

Corresponding author: T. Cavailhes, Badley Ashton & Associates Ltd., Winceby Ho Horncastle LN9 6PB, United Kingdom. (Thibaultcavailhes@badley-ashton.co.uk)

©2013. American Geophysical Union. All Rights Reserved.
0094-8276/13/10.1002/grl.50829

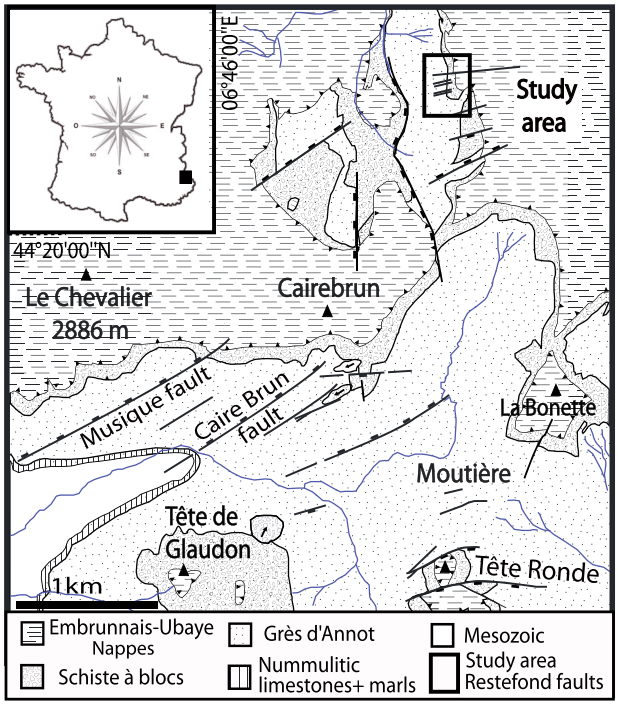

Figure 1. Structural sketch of the study area: the studied N080–100E Restefond faults were active at temperature about 200°C (see text).

3. Fault Zone Macrostructures

[5] The studied faults are three minor normal faults located in the damage zone of the Restefond fault, which belongs to a set of normal faults of decameter offset cutting the upper part of the Gres d'Annot formation (GAF). The GAF surrounding the Restefond fault is a subhorizontal succession composed by up to several meters-thick arkosic sandstone beds and decimeter-thick pelitic intercalations. The three studied faults trend about N090E; they have subvertical dips and show their own damage zones a few centimeters thick and composed of quartz-filled fractures (Figure 2a). The fault core zones, a few millimeters thick, exhibit a macroscopic mineralogical fabric (foliation) defined by alternating phyllosilicate and quartz layers tilted in S-C structures (see below: fault zone microstructures).

[6] On the three studied faults, normal displacement ranges from 20 to 110 cm, which is less than the thickness of the sampled arkosic layers. This eliminates the possibility of mechanical incorporation of phyllosilicates by smearing/abrasion during sliding past pelite layers. This geometrical configuration allows us to better characterize the formation of phyllosilicates related to synkinematic or post-kinematic fluid-rock interactions in the studied fault zones.

4. Fault Zone Microstructures

[7] The host rocks are poorly sorted, fine- to coarse-grained arkosic sandstones mainly composed of quartz, K-feldspar, plagioclase, and phyllosilicate (biotite, white micas, and chlorite). All the different types of feldspars are moderately altered in white micas of 20–60 µm in size in relation to the intense diagenesis; they are distributed following the cleavage planes and at the boundaries of the feldspar grains. The high diagenesis grade is also marked by strong imbrication of grains by pressure solution and quartz-sealed intragranular extensional microfractures.

[8] The fault core (or fault rock) is characterized by a millimeter-thick zone of foliated and damaged arkose showing grain size reduction acquired by grain fracturing (Figure 2b); their mineralogical foliation results from the fabric of quartz and feldspars given by (i) a pronounced stylolitisation at the grain contacts parallel to the grain long axes and (ii) closely spaced intragranular extensional microfractures subperpendicular to the stylolitized grain contacts (Figure 2b). The numerous anastomosed stylolites follow the shapes of the normal shears marked by the foliation and defining an S-C fabric. The microfractures in the quartz grains are mainly sealed by authigenic quartz and in the feldspar grains, by small white micas (20–60 µm, see Figures 2b–2g). The foliation shows a passive concentration of newly formed phyllosilicates associated with disaggregated altered feldspar grains (all types and all sizes) and intensely stylolitized and microfractured quartz grains. These newly formed phyllosilicates are mainly well-connected small white micas of phengitic composition and subsidiary chlorite (Figures 2c–2g) [*Leclère et al.*, 2012]. At the grain scale, these white micas are localized (i) within feldspar grains, dispersed along the cleavage planes, (ii) within fractures and shear zones damaging feldspar grains along the cleavage planes, and (iii) along the surfaces of feldspar fragments disaggregated by intense brittle fracturing (Figures 2f–2g). Where the deformation is more advanced, the synkinematic newly formed micas are preferentially more abundant near relict feldspar grains and have commonly sigmoidal shapes kinematically consistent with S-C structures (Figure 2d). The precipitation of synkinematic chlorite, intermixed in stack shape with white micas, always occurs in mature shear zones (Figure 2d).

5. Quantifying Phyllosilicate Proportion

[9] Hydraulic and mechanical properties of fault zones are closely linked to the mineralogical composition and properties of fault rocks. Here, we aim to compare the initial mineralogy of the host rock, considered as the protolith (see above), and the fault rock in order to discuss the proportions of mineralogical changes. We have counted the number of mineral grains, with a counting step of 0.3 mm, along scan lines spaced by 0.3 mm and parallel to the main slip plane. In the nine host rock thin sections, 7200 points have been counted. In the 17 foliated fault rock thin sections, cut along the *X-Z* deformation axes [*Ramsay*, 1967], 3709 points have been counted (Table 1).

[10] The homogeneous mineralogical composition of host rock corresponds to an arkose of mean composition $Q_{57–62}\,F_{35–41}\,Phyl._{1–3}$ (Figure 3). The fault rock composition is nearly constant between the samples, with the following proportions: $Q_{55–61}\,F_{5–12}\,Phyl_{26–35}$ (Figure 3; Table 1). Compared to the host rock values, the content of quartz remains nearly unchanged, whereas a larger content of phyllosilicate balances a loss of feldspar. Indeed, in the ternary diagram, the vector of mineralogical variations between the host rocks and fault rocks compositions is subparallel to the feldspar-phyllosilicate axis (Figure 3). It is also worth to note that there is no correlation between the proportion of newly formed phyllosilicates and fault offset (Figure 3). This point shows that the large proportion of newly formed phyllosilicates

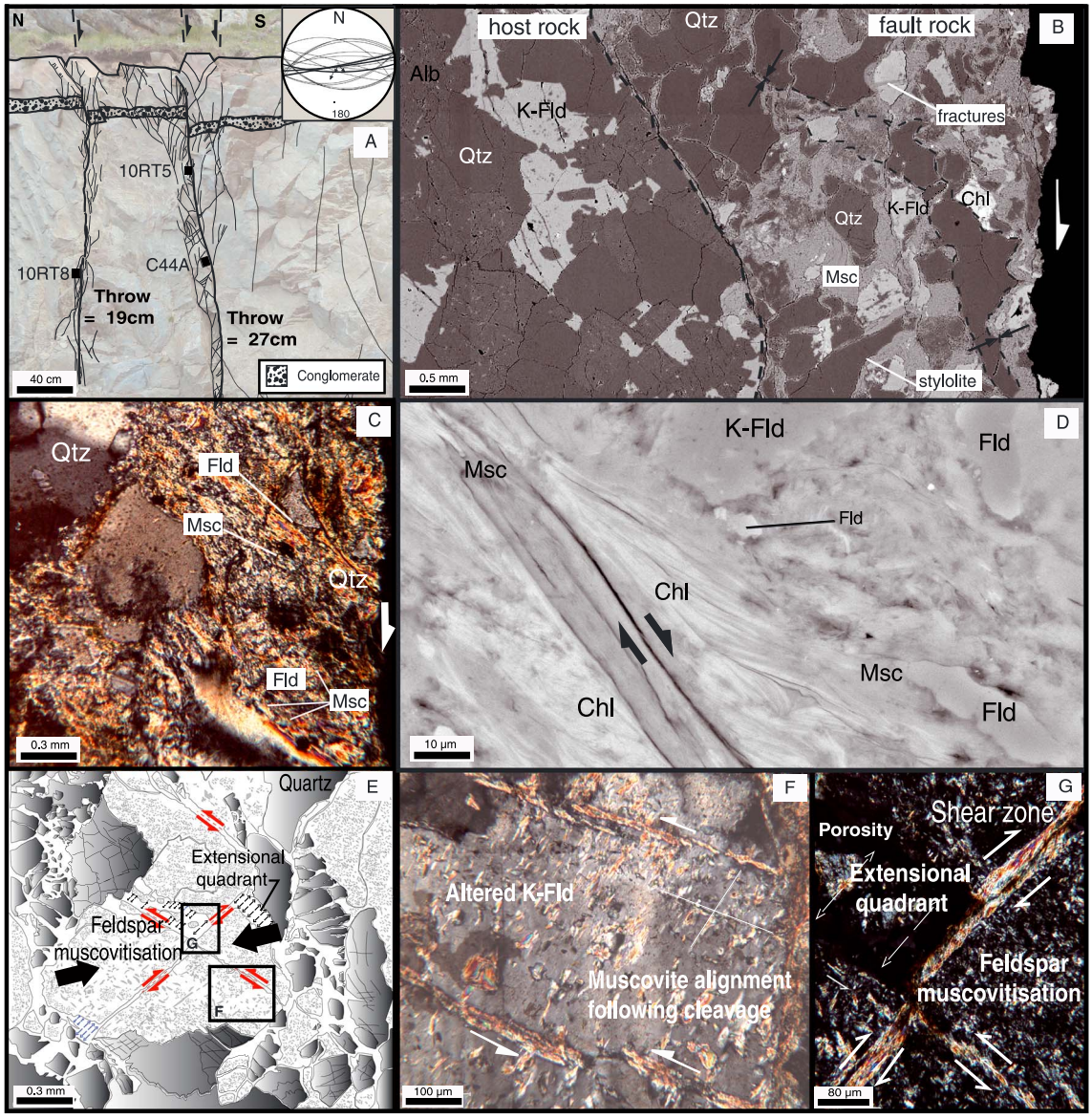

Figure 2. (a) Stereogram and general view of two of the three studied faults, with location of samples (10RT8, C44A, and 10RT5). (b) Microscopic view of the arkosic host rock and foliated fault rock. (c) Optical microscopic view (polarized light) of the fault rock showing the foliation underlined by abundant preferentially oriented muscovites (sample 10RT8). (d) Micro-shear zone mainly composed of chlorite and muscovite defining an S-C structure, whereas feldspar fragments are preserved at the periphery of the shear zone (sample 10RT8, back-scattered scanning electron microscope image). (e) Drawing of the initiation of brittle fracturing and alteration of feldspar grains (sample 10RT5). (f, g) Microscopic view (polarized light) of Figure 2e showing reactional surfaces underlined by muscovite along cleavage planes. Qtz: Quartz, Fld: Feldspar, Alb: Albite, Msc: Muscovite, Chl: Chlorite.

(around 30% of the fault rock volume) in the studied fault rocks has been acquired at the initiation of the faults (i.e., for a normal offset less than 20 cm) and remains about the same for larger offset (110 cm).

6. Discussion

[11] The two possible reasons for a high proportion of phyllosilicates (and related mechanical/hydraulic properties) in fault zones are (i) mechanical incorporation of detrital phyllosilicates from the host rock and (ii) diagenetic/metamorphic reactions. In the case studied here, the location of the samples, i.e., faults offset limited to arkosic beds, implies that the initial host rock could not supply a large proportion of detrital phyllosilicates to the fault rock. On the other hand, microstructural observation shows that synkinematic muscovitisation of feldspars disaggregated by brittle fracturing was active in these fault zones from the upper crust (Figures 2c–2e). This shows that the presence of phyllosilicates in the fault rock results from feldspar alteration under hydrous conditions (see equations in *Wibberley* [1999]). From the microstructural analysis, we assume that this supply of phyllosilicates in the present day fault rocks is related to the brittle deformation within the fault in a pressure temperature context (i.e., 200°C, 6–7 km of depth, in presence of water) that enhances feldspar alteration.

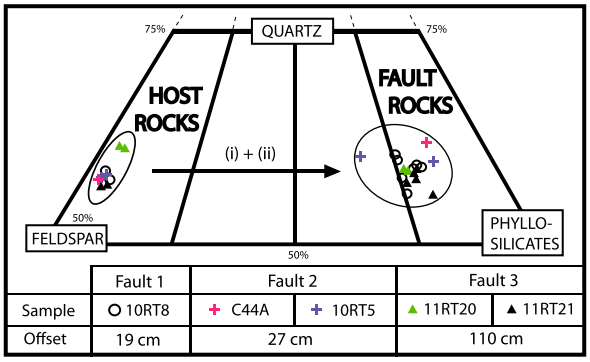

Figure 3. Host rock and fault rock compositions determined by point counting, shown in a ternary diagram for feldspar, quartz, and phyllosilicates. The arrow highlights the mineralogical change between the host rocks and the fault rocks.

6.1. Degree of Feldspar Alteration

[12] The discussion above implies that understanding the potential variability of the feldspar-to-phyllosilicate transformation is critical to estimate the phyllosilicate proportion in fault rocks. In our case, we observe a decrease of ~80% of feldspar proportion between the initial host rock and the fault rock compositions (see Table 1). It has been shown that feldspar alteration requires presence of aqueous fluids and depends on several parameters including (1) the P-T conditions, which can activate or inhibit muscovitisation [*Hunziger*, 1986; *Chardon et al*., 2006], (2) the fluid chemistry and duration of alteration [*Chardon et al*., 2006], (3) coating of feldspar grains by hydrocarbons which protect feldspar from alteration [*Strovoll et al*., 2002], (4) the nature of the feldspar altered (K or Na feldspar) and the phyllosilicate formed [*Kamineni et al*., 1993; *Chardon et al*., 2006], and also probably (5) the style of deformation (displacement, creep versus seismic, and effective stress). Although points (1) to (4) cannot be tested in this study and remain to be constrained, it appears clear that the amount of slip has no influence on the amount of transformation in the studied examples; there is no correlation between the proportion of newly formed phyllosilicates and fault offset (Figure 3). This suggests that feldspars were transformed into phyllosilicates at the initiation of the faulting, i.e., for slip less than 20 cm, or subsequently after initiation, using the reactional surfaces newly formed by grain fracturing in the presence of water. Incipient comminution of feldspar during fault initiation provides a high number of reactional surfaces and enhances the process of white mica formation [e.g., *Wibberley*, 1999]. Thereby, this process seems potentially more developed in P-T conditions comprised between the temperature of feldspar muscovitisation activation (i.e., ~200°C) [*Hunziger*, 1986], and the temperature below which feldspar is "brittle," which could critically enhance the mineral transformation process (increasing reactive surfaces, i.e., 450°C) [*Passchier and Trouw*, 2005].

[13] Assuming that there is no loss or supply of elements during alteration, we infer that ~80% of initial feldspar content was transformed into phyllosilicates during diagenesis-assisted faulting. Although such migration of elements cannot be excluded along faults [e.g., *Wibberley and McCaig*, 1999], Figures 2e–2g shows that feldspar dissolution and phyllosilicate precipitation are in situ processes related to incipient brittle fracturing. Such a context of small-scale deformation suggests that migration (i.e., advection of water) should be very local, restricted to the process zone at fault fracturing initiation. We therefore infer that the proportion of phyllosilicates in the fault rock mainly depends on the initial proportion of feldspars in the host rock and the proportion of them being transformed into phyllosilicates (vector in Figure 3).

6.2. Phyllosilicate Content and Implications for Fluid Flow

[14] In order to discuss the proportion of phyllosilicates in the fault rock and its impact on fluid flow, we compare our results to the Shale Gouge Ratio (SGR) algorithm commonly used to predict the phyllosilicate proportion in fault rocks [e.g., *Yielding*, 2002]. The SGR algorithm is expressed as

$$\mathrm{SGR} = \frac{\sum(\mathrm{Er} \times \Delta\ \mathrm{shale})}{\mathrm{Throw}} \quad (1)$$

where (Throw) is the vertical component of the dip-slip offset, Er is the thickness of a layer of host rocks cut by the fault containing a specific clay fraction, and (Δ shale) is the specific clay fraction of the layer considered (see *Yielding* [2002] for more details). Applying this conventional method to our data yields an SGR of 1 to 3%, which is equal to the phyllosilicate content of the arkosic host beds because the throw is less than bed thickness. This is much lower than the phyllosilicate content measured in the fault rock samples (25–34%) (Figure 4a). Because the proportion of detrital phyllosilicates is negligible in our case, replacing Δ shale by Δ feldspar in equation (1) provides the maximum possible proportion of neoformed phyllosilicates (~40%).

[15] It is worth to note that synkinematic phyllosilicate formation by feldspar muscovitisation is not possible at shallow depths (A in Figure 4b), where the mechanical incorporation is prominent. Below a depth approximately corresponding to the 200°C isotherm [*Hunziger*, 1986], both mechanical incorporation and synkinematic feldspar alteration are possible (from B to C in Figure 4b). In such case, faults could contain more than 20% of phyllosilicates and be considered as membrane seals in deeply buried porous reservoir [*Yielding*, 2002] (Figure 3). In low-porosity rocks, phyllosilicates in faults favor drain parallel to the *Y* principal direction of deformation [e.g., *Cavailhes et al*., 2013] and also can trap fluid pressure increases and reduce normal stress, which in addition to their low frictional coefficient, their size and their connectivity, can drastically reduce fault strength [e.g., *Wibberley and Shinamoto*, 2005; *Lockner et al*., 2011].

7. Conclusion

[16] We show that even in such a relatively low-grade metamorphism and small-displacement (a few tens of centimeters) faulting context, that brittle deformation and alteration of feldspar under hydrated conditions can induce alteration to generate phyllosilicates contributing to around 25% to 34% of the fault rock volume, derived from a protolith comprising about 40% of feldspar and less than 3% of detrital phyllosilicates. The synkinematic or post-kinematic timing of this alteration suggests that only fault rocks alteration active at temperatures between 200° and 450° in such crushed quartzofeldspathic rocks should have such a significant alteration-related phyllosilicate content. Given the very small

Table 1. Results for Data of Point Counting for 9 Thin Sections of Host Rocks and 17 Thin Sections of Fault Rocks[a]

Sample	Offset of the Studied Fault (cm)	Quartz		Feldspar		Detrital Phyllosilicates		Total Phyllosilicates		Theorical Value (%) Computed by SGR	Proportion of Disappeared Feldspar Between HR and FR
		Points	Percent	Points	Percent	Points	Percent	Points	Percent		
10RT8Hostrock1	19	458	57.25	318	39.75	24	3	24	3	3	Not relevant
10RT8Hostrock2	19	467	58.37	322	40.25	11	1.38	11	1.38	1.38	Not relevant
10RT8A	19	128	59.27	16	7.40	5	2.31	67	31.02	$1.38 < SGR < 3$	0.81
10RT8B1	19	142	59.16	21	8.75	7	2.92	70	29.17	$1.38 < SGR < 3$	0.78
10RT8B2	19	173	57.67	31	10.33	9	3	87	29	$1.38 < SGR < 3$	0.74
10RT8C1	19	159	60.22	26	9.86	7	2.65	72	27.27	$1.38 < SGR < 3$	0.75
10RT8C2	19	134	55.83	26	10.84	7	2.91	73	30.42	$1.38 < SGR < 3$	0.73
10RT8D1	19	118	61.46	18	9.38	3	1.56	53	27.6	$1.38 < SGR < 3$	0.76
10RT8D2	19	156	59.09	20	7.58	4	1.51	84	31.82	$1.38 < SGR < 3$	0.81
10RT5Hostrock1	27	464	58	323	40.47	13	1.63	13	1.63	1.63	Not relevant
10RT5Hostrock2	27	461	57.62	327	40.88	12	1.5	12	1.5	1.5	Not relevant
10RT5A	27	191	60.25	19	5.95	4	1.26	103	32.49	$1.5 < SGR < 1.63$	0.85
10RT5B	27	89	60.95	18	12.32	2	1.36	37	25.34	$1.5 < SGR < 1.63$	0.69
C44Hostrock	27	456	57	335	41.89	9	1.11	9	1.11	1.11	Not relevant
C44A	27	123	64.06	10	5.2	0	0	59	30.72	1.11	0.87
10RT20Hostrock1	110	497	62.12	286	35.75	17	2.13	17	2.13	2.13	Not relevant
10RT20Hostrock2	110	501	62.63	285	35.62	14	1.75	14	1.75	1.75	Not relevant
10RT20A	110	86	58.5	14	9.52	3	2.04	44	29.93	$1.75 < SGR < 2.13$	0.73
10RT20B	110	109	58.82	18	9.79	3	1.93	56	30.35	$1.75 < SGR < 2.13$	0.72
10RT21Hostrock1	110	459	57.37	322	40.25	19	2.38	19	2.38	2.38	Not relevant
10RT21Hostrock2	110	449	56.12	330	41.26	21	2.62	21	2.62	2.62	Not relevant
10RT21A	110	81	56.64	11	7.69	3	2.09	48	33.56	$2.38 < SGR < 2.62$	0.81
10RT21B	110	128	58.71	18	8.25	2	0.91	70	32.11	$2.38 < SGR < 2.62$	0.79
10RT21C	110	97	57.73	15	8.92	3	1.78	53	31.54	$2.38 < SGR < 2.62$	0.78
10RT21D	110	134	57.27	23	9.83	6	2.56	71	30.34	$2.38 < SGR < 2.62$	0.76
10RT21E	110	142	58.67	19	7.85	6	2.47	75	30.99	$2.38 < SGR < 2.62$	0.8

[a]HR: host rock, FR: fault rock, Det: percentage of detrital phyllosilicates within the studied rocks.

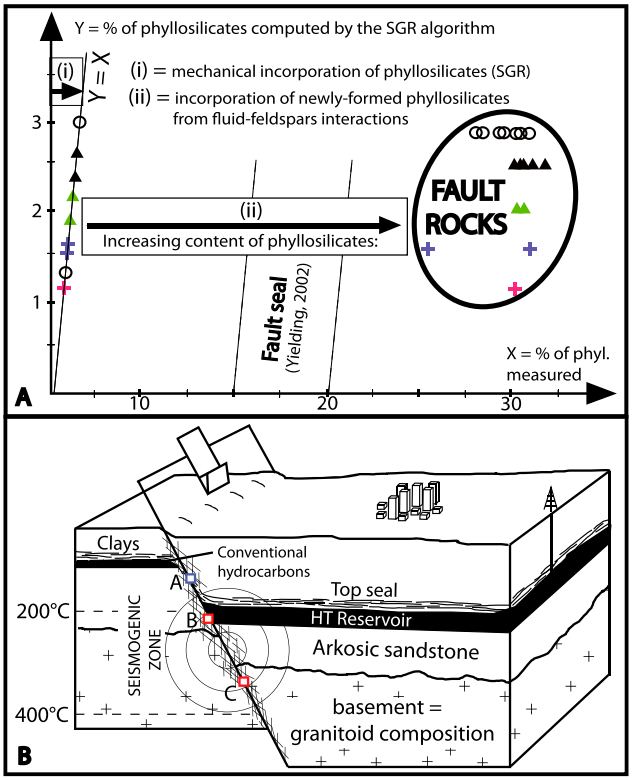

Figure 4. (a) Comparison of the amounts of phyllosilicates calculated using the SGR algorithm with the measured phyllosilicate contents (see equation (1) in the text). Note that the mechanical fault seal effect predicted by equation of *Yielding* [2002] (mica content of 3%) is well below the observed mica content (30%) derived from feldspar alteration. (b) Summary of the importance of phyllosilicate mechanical incorporation versus formation derived from feldspar alteration as a function of depth, temperature, and lithology. See explanations in *Phyllosilicate content and implications for fluid flow* part.

displacement necessary for grain-crushing enhancing such alteration, the maximum phyllosilicate content (to which sealing capacity or fault strength can be related) of any such fault affecting a quartzofeldspathic protolith under very low-grade metamorphism conditions can be predicted from the feldspar content of the host rock.

[17] **Acknowledgments.** We thank the oil and gas company TOTAL for financial support. Jean-Pierre Gratier, Andrew Newman, and anonymous reviewers are acknowledged for their constructive reviews which have considerably contributed to improve the quality of this paper.

[18] The Editor thanks Jean-Pierre Gratier and an anonymous reviewer for their assistance in evaluating this paper.

References

Bradbury, K. K., J. P. Evans, J. S. Chester, F. M. Chester, and D. L. Kirschner (2011), Lithology and internal structure of the San Andreas fault at depth based on characterization of Phase 3 whole-rock core in the San Andreas Fault Observatory at Depth (SAFOD) borehole, *Earth Planet. Sci. Lett.*, *310*, 131–144, doi:10.1016/j.epsl.2011.07.020.

Cavailhes, T., et al. (2013), Influence of fault rock foliation on fault zone permeability: The case of deeply buried arkosic sandstones (Grès d'Annot, SE FRANCE): American Association of Petroleum Geologists Bulletin, AAPG Bulletin, *97*(7), 1521–1543, doi:10.1306/03071312127.

Chardon, S. E., R. F. Livens, and D. J. Vaughan (2006), Reactions of feldspar surfaces with aqueous solutions, *Earth Sci. Rev.*, *78*, 1–26.

Di Toro, G., R. Han, T. Hirose, N. De Paola, S. Nielsen, K. Mizoguchi, F. Ferri, M. Cocco, and T. Shinamoto (2011), Fault lubrication during earthquakes, *Nature*, *471*, 494–499, doi:10.1038/nature09838.

Evans, P. E. (1990), Textures, deformation mechanisms, and the role of fluids in the cataclastic deformation of granitic rocks, in *Deformation Mechanisms, Rheology and Tectonics,* vol. 54, edited by R. J. Knipe and E. H. Rutter, pp. 29–39, Geological Society of London, special publications, London, doi:10.1144/GSL.SP.1990.054.01.03.

Faulkner, D. R., C. A. L. Jackson, R. J. Lunn, R. W. Schlische, Z. K. Shipton, and C. A. J. Wibberley (2010), A review of recent developments concerning the structure, mechanics and fluid flow properties of fault zones, *J. Struct. Geol.*, *32*, 1557–1575, doi:10.1016/j.jsg.2010.06.009.

Fisher, Q., and R. J. Knipe (2001), The permeability of faults within siliclastic petroleum reservoirs of the North Sea and Norwegian Continental Shelf, *Mar. Pet. Geol.*, *18*, 1063–1081.

Fisher, Q., J. M. Casey, S. D. Harris, and R. J. Knipe (2003), Fluid flow properties of faults in sandstone: The importance of temperature history, *Geology*, *31*, 965–968.

Gapais, D. (1989), Shear structures within deformed granites: Mechanical and thermal indicators, *Geology*, *17*, 1144–1147.

Haines, S. H., and B. A. van der Pluijm (2012), Patterns of mineral transformations in clay gouge, with examples from low-angle normal fault rocks in the western USA, *J. Struct. Geol.*, *43*, 2–32.

Hunziger, J. C. (1986), The evolution of illite to muscovite: An example of the behavior of isotopes in low-grade metamorphic terrains, *Chem. Geol.*, *57*, 31–40.

Janecke, S. U., and P. E. Evans (1988), Feldspar-influenced rock rheologies, *Geology*, *16*, 1064–1067.

Joseph, P., and S. A. Lomas (2004), *Deep water sedimentation in the Alpine Foreland Basin of SE France: A new perspective on the Grès d'Annot and related systems*, Geological Society, special publication, vol. *211*, pp. 1–16, London, United Kingdom.

Kamineni, D. C., R. Kerrich, and A. Brown (1993), Effects of differential reactivity of minerals on the development of brittle to semi-brittle structures in granitic rocks: Textural and oxygen isotope evidence, *Chem. Geol.*, *105*, 215–232.

Kerckhove, C. (1969), La < zone du flysch > dans les nappes de l'Embrunais-Ubaye (Alpes occidentales), *Géologie Alpine*, *45*, 1–202.

Labaume, P., M. Jolivet, F. Souquière, and A. Chauvet (2008), Tectonic control on diagenesis in a foreland basin: Combined petrologic and thermochronologic approaches in the Grès d'Annot basin (Late Eocene-Early Oligocene, French-Italian external Alps), *Terra Nova*, *20*, 95–101, doi:10.1111/j.1365-3121.2008.00793.x.

Labaume, P., et al. (2009), Diagenesis controlled by tectonic burial in a foreland basin turbidite formation. The case example of the Grès d'Annot, French-Italian external Alps: Geophysical Research Abstracts, 11, EGU2009-8236-3, EGU General Assembly 2009, Vienna.

Leclère, H., M. Buatier, D. Charpentier, J.-P. Sizun, P. Labaume, and T. Cavailhes (2012), Formation of phyllosilicates in fault zone affecting deeply buried arkosic sandstones. Their influence on fault zone petrophysic properties (Annot sandstones, French external Alps), *Swiss J. Geosci.*, doi:10.1007/s00015-012-0099-z.

Lockner, D., C. Morrow, D. Moore, and H. Stephen (2011), Low strength of deep San Andreas fault gouge from SAFOD core, *Nature*, *472*, 82–86, doi:10.1038/nature09927.

Maggi, A., J. A. Jackson, D. McKenzie, and K. Priestley (2000), Earthquake focal depths, effective elastic thickness, and the strength of the continental lithosphere, *Geology*, *28*, 495–498.

Mitra, G. (1978), Ductile deformation zones and mylonites: The mechanical processes involved in the deformation of crystalline basement rocks, *Am. J. Sci.*, *278*, 1057–1084.

Moore, D. E., and J. D. Byerlee (1989), Textural development of clayey and quartzofeldspathic fault gouges relative to their sliding behavior, *Phys. Chem. Earth*, *17*, 1–9.

Mullis, J., K. M. Rahn, P. Schwer, C. Capitani, W. B. Stern, and M. Frey (2002), Correlation of fluid inclusion temperatures with illite "crystallinity" data and clay mineral chemistry in sedimentary rocks from the external part of the Central Alps, *Schweiz. Mineral. Petrogr. Mitt.*, *82*, 325–340.

Passchier, C. W., and R. A. J. Trouw (2005), *Microtectonics*, Springer, Berlin, pp. 1–366.

Ramsay, J. G. (1967), *Folding and Fracturing of Rocks*, McGraw-Hill Book Company, New York, pp. 1–560.

Scholz, H. C. (1990), *The Mechanics of Earthquakes and Faulting*, Cambridge University Press, New York, pp. 439.

Strovoll, V., K. Bjorlykke, D. Karlsen, and G. Saigal (2002), Porosity preservation in reservoir sandstones due to grain-coating illite: A study of the Jurassic Garn Formation from the Kristin and Lavrans fields, offshore Mid-Norway, *Mar. Pet. Geol.*, *19*, 767–781.

Wibberley, C. A. J. (1999), Are feldspar-to-mica reactions necessarily reaction-softening processes in fault zones?, *J. Struct. Geol.*, *21*, 1219–1227.

Wibberley, C. A. J., and A. McCaig (1999), Quantifying orthoclase and albite muscovitisation sequences in fault zones, *Chem. Geol.*, *165*, 181–196.

Wibberley, C. A. J., and T. Shinamoto (2005), Earthquake slip weakening and asperities explained by thermal pressurization, *Nature*, *436*, 689–692, doi:10.1038/nature03901.

Yielding, G. (2002), *Shale Gouge Ratio—Calibration by Geohistory*, in A.G. Koeslter and R. Hunsdale, eds, hydrocarbon seal quantification: Norwegian Petroleum Society Special Publication, *11*, pp. 1–15.